

Topological Methods for Polymeric Materials: Characterizing the Relationship Between Polymer Entanglement and Viscoelasticity.

Eleni Panagiotou[#], Ken Millett[#], and Paul J. Atzberger^{#,§ *}

[#]Department of Mathematics, University of California Santa Barbara, CA 93106-3080

[§]Department of Mechanical Engineering, University of California Santa Barbara, CA 93106-3080

*e-mail: atzberger@gmail.com; website: <http://atzberger.org/>

January 27, 2023

We draw on mathematical results from topology to develop quantitative methods for polymeric materials to characterize the relationship between polymer chain entanglement and bulk viscoelastic responses. We generalize the mathematical notion of the Linking Number and Writhe to be applicable to open (linear) chains. We show how our results can be used in practice by performing fully three-dimensional computational simulations of polymeric chains entangled in weaves of a few distinct topologies and with varying levels of chain densities. We investigate relationships between our topological characteristics for chain entanglement and viscoelastic responses by performing Lees-Edwards simulations of the rheology over a broad range of frequencies. Our topological measures of entanglement indicate the global topology is the dominant factor in characterizing mechanical properties. We find an almost linear relation between the mean absolute Writhe Wr and the loss tangent and an almost inverse linear relation between the mean absolute Periodic Linking Number LK_P and the loss tangent. These results indicate the potential of our topological methods in providing a characterization of the level of chain entanglement useful in understanding the origins of mechanical responses in polymeric materials.

1 Introduction

A fundamental problem in material science is to understand the relationship between molecular-level interactions and resulting bulk material properties. We consider polymeric materials and develop mathematical approaches for investigating the relationship between topology of the polymeric chains and bulk viscoelastic mechanical responses. A key feature is the nature of the entanglements that arise between polymeric chains from the inherent sterics of the polymers comprising the material. The collective configurations of the chains can result in complex entangled structures that greatly restrict chain motions and transmission of mechanical stresses within the material [11, 12, 53]. Characterizing these intuitive physical notions in a quantitatively precise mathematical way poses a number of interesting and significant challenges. In practice entangled polymer melts or gels often involve kinetics over a broad range of time-scales with collective responses that often depend on both the frequency and duration of mechanical perturbations. In addition, the polymer chains often exhibit friction with respect to one another or coupling from immersion within a solvent fluid that can result in varied viscoelastic responses that may show a significant frequency dependence [2–4, 64].

A common approach to entanglement involves considering two different length and time scales. First, there is the length scale of the entire chain, where global entanglement occurs as the chains get knotted and linked to each other [5, 12–14, 28, 29]. Second, one has local entanglement arising from the local constraints, obstacles, that a chain feels at a small length scale. This length scale, also called the entanglement length, plays an important role in models of entangled polymer dynamics and is related to the tube diameter in tube model theories [24, 31, 53, 56, 58]. The relation between these two is poorly understood. Even experimentally, different methods for the determination of the plateau modulus and the entanglement molecular weight can give different results [37]. Since Edwards’ tube model, several improvements of this theory have emerged, but inconsistencies are still present [18, 35]. Moreover, an even shorter length scale, that of the packing length, has been shown to have an influence and should be incorporated in theories of polymer viscoelasticity [63].

The relation between entanglement and viscoelastic properties of materials has been studied indirectly by varying the density or molecular weight of the chains and, therefore, varying the number of contacts between neighboring chains [20, 27, 30, 54, 62]. A measure of entanglement that is very helpful in the study of polymers is the number of kinks per chain. This is a quantity that is usually derived from the application of a contour reduction algorithm on a polymer melt [7, 20, 30, 62]. However, the global entanglement complexity cannot be assessed by only measuring the number of contacts. This has led to the use of tools from knot theory to study entanglement in polymers [13, 14, 19–21, 32, 50]. The difficulty in using tools from knot theory is that they are defined on simple closed curves in space (rings) while the polymer chains can have various architectures, often those of linear chains. In order to deal with this, a statistical definition of knotting has been introduced [39]. This method can determine the principal knot type of a fixed configuration of an open chain. However, the polymer chains move in time and this method may have problems when applied to study entanglement in non-equilibrium conditions. Moreover, the tools from knot theory cannot yet be applied to systems employing three-dimensional Periodic Boundary Conditions (PBC) since the corresponding theory is missing [42].

In this study, we take another complimentary approach where we use mathematical ideas from topology and geometry to provide additional quantities we refer to as the collective “linking number” and “Writhe” to quantify the level of polymer entanglement complexity [44–46]. The advantage of the Gauss linking integral is that it can be applied to both linear and ring polymers and it is a continuous function of the chain coordinates. Moreover, in [44] it has been shown that it can be extended to systems with 1, 2 or 3 PBC to provide a new continuous measure of entanglement. These measures have been applied to both equilibrium and non-equilibrium conditions. More precisely, our proposed measures have been used to understand the disentanglement of chains and to provide a new estimator of the entanglement length which indicates they can be useful in polymer theories [45–47]. In order to incorporate these measures in theories of polymer entanglement, input of atomistic simulations for the interplay between applied deformation and system structure is required. In this work measures from topology and geometry are used to understand the interplay between entanglement and mechanics. In particular, they are applied to the viscoelastic mechanical responses of the polymeric material.

We carry-out our studies of mechanical response by using a precisely controlled global topology that we then vary. Our computational model consists of polymeric chains represented by bonded steric beads having Weeks-Chandler-Andersen (WCA) interactions and harmonic bonds. We simulate a sample of the polymeric material using a model based on three-dimensional PBC with our fixed

global topology arising from the chains extending through the boundary of the periodic box. We also simulate corresponding systems whose topology is allowed to vary by considering weaves composed by short linear polymer chains. We examine the mechanical response of such systems ranging from weakly entangled to strongly entangled under oscillatory shear deformation (Lees-Edwards boundary conditions [33]) and report the local and global entanglement effects measured using our topological tools. All computational simulations were performed using the LAMMPS molecular dynamics package and our custom extension packages (<http://lammps.sandia.gov>).

We organize the paper as follows. In Section 2 we introduce tools from knot theory to precisely characterize the topology of the polymeric chains. In Section 3 we describe a class of polymeric materials based on weave-like topologies that we consider throughout our investigations. In Section 4, we discuss the details of our computational methods and simulation approaches. In Section 5, we present our results and discuss interesting features of the relationship between polymer entanglement and bulk material response.

2 Characterizing Polymer Entanglement

We measure the degree to which polymer chains interwind and attain complex configurations using the Gauss linking integral:

Definition 2.1. (Gauss Linking Number). The Gauss *Linking Number* of two disjoint (closed or open) oriented curves l_1 and l_2 , whose arc-length parametrizations are $\gamma_1(t), \gamma_2(s)$ respectively, is defined as the following double integral over l_1 and l_2 [23]:

$$L(l_1, l_2) = \frac{1}{4\pi} \int_{[0,1]} \int_{[0,1]} \frac{(\dot{\gamma}_1(t), \dot{\gamma}_2(s), \gamma_1(t) - \gamma_2(s))}{\|\gamma_1(t) - \gamma_2(s)\|^3} dt ds, \quad (1)$$

where $(\dot{\gamma}_1(t), \dot{\gamma}_2(s), \gamma_1(t) - \gamma_2(s))$ is the *scalar triple product* of $\dot{\gamma}_1(t), \dot{\gamma}_2(s)$ and $\gamma_1(t) - \gamma_2(s)$.

This can also be expressed alternatively in terms of line integration as

$$L(l_1, l_2) = \frac{1}{4\pi} \oint \oint \frac{\gamma_1(t) - \gamma_2(s)}{\|\gamma_1(t) - \gamma_2(s)\|^3} \cdot (d\gamma_1(t) \times d\gamma_2(s)). \quad (2)$$

The Gauss Linking Number is a topological invariant for closed chains and a continuous function of the chain coordinates for open chains.

We also define a one chain measure for the degree of intertwining of the chain around itself:

Definition 2.2. (Writhe). For a curve ℓ with arc-length parameterization $\gamma(t)$ is the double integral over l :

$$Wr(l) = \frac{1}{4\pi} \int_{[0,1]} \int_{[0,1]} \frac{(\dot{\gamma}(t), \dot{\gamma}(s), \gamma(t) - \gamma(s))}{\|\gamma(t) - \gamma(s)\|^3} dt ds. \quad (3)$$

The Writhe is a continuous function of the chain coordinates for both open and closed chains.

For systems employing Periodic Boundary Conditions (PBC), the linking that is imposed from one simulated chain on another chain propagates in three dimensional space by the images of the other chain. In other words, for a system with PBC each simulated chain gives rise to a *free chain* in the periodic system which consists of an infinite number of copies of the simulated chain. We call

each copy of a chain an *image* of the free chain. It has been shown that a measure of entanglement that can capture the global linking in a periodic system is the *periodic linking number* LK_P [44]:

Definition 2.3 (Periodic Linking Number). Let I and J denote two (closed, open or infinite) free chains in a periodic system. Suppose that I_u is an image of the free chain I in the periodic system. The *Periodic Linking Number*, LK_P , between two free chains I and J is defined as:

$$LK_P(I, J) = \sum_v L(I_u, J_v), \quad (4)$$

where the sum is taken over all the images J_v of the free chain J in the periodic system.

The Periodic Linking Number is a topological invariant for closed chains and a convergent series for open chains that changes continuously with the chain coordinates. For its computation, we use a cutoff, the *local Periodic Linking Number* [44, 47].

3 Polymeric Materials with Weave-like Entanglements

We study polymeric materials having a few different initial topologies. We make two specific distinctions between when the global topology is fixed and when the global topology can change. We consider four distinct types of polymeric materials having polymeric chains with topological structures corresponding to different types of weaves. For each of these materials, we vary their entanglement conformation and density. We do this for each of two different architectures corresponding to either infinite or open chains.

The infinite chains have no endpoints inside the simulation box and, therefore, extend periodically throughout the simulation to create an infinite weave. The open chains also cross the periodic boundary but have distinct starting and endpoints, thereby creating an open weave. The weave complexity ranges from trivial (w0), orthogonal non-interlaced at different densities (wI, wII) and alternating interlacing (wIII). For details see Table 1 and Figures 1, 2. The weave w0 has trivial global topology. The weaves wI and wII have the same global topology. The weave wIII has the same density as wII, but it has non-trivial global topology, more complex than that of wII.

The open systems are created by deleting one bond from each chain in the simulation box in the original conformation and the infinite and corresponding open systems start from the same original conformations (except for one bond). Due to the uncrossability constraint, the global topology of the infinite systems cannot change without breakage of the bonds, while the global topology of the systems of open chains can change by slippage of the chains past entanglements. Notice that in both infinite and open cases, the local geometry and topological constraints of the chains can change.

By subjecting the material to oscillatory shear deformations, we can measure the extent the density or the topological complexity affect mechanical responses. Concerning the use of polymeric weave configurations, let us note that, in addition to providing a simple characterization of polymer entanglement for the purpose of this study, they also appear in the study of metal organic frameworks and crystals (see [17] and references therein).

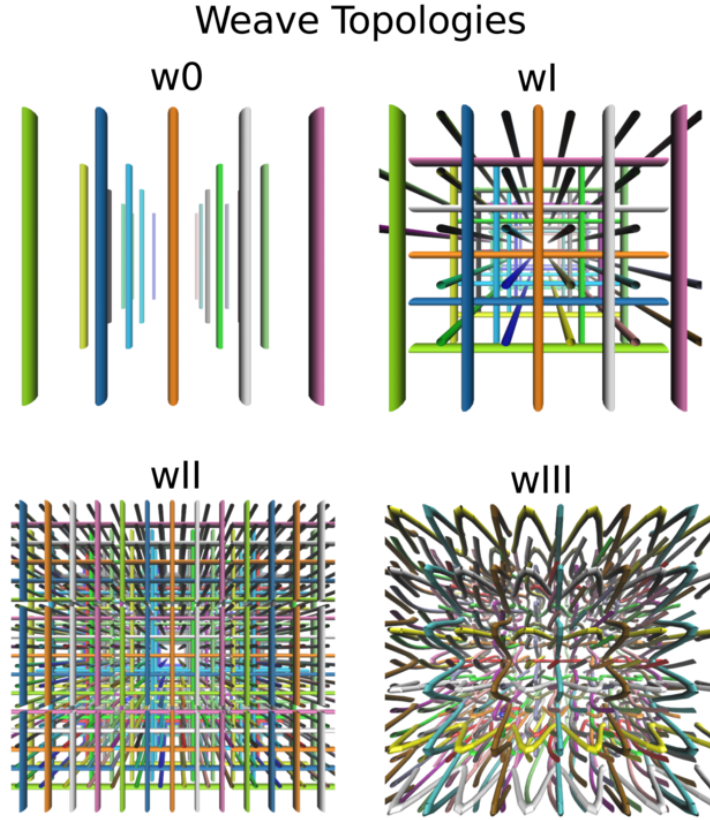


Figure 1: The different weaves we consider in our studies labelled as *weave0* (*w0*), *weaveI* (*wI*), *weaveII* (*wII*) and *weaveIII* (*wIII*). Shown from top (left to right), bottom (left to right).

Weave	Topology	Density	MW (open)
Weave 0 (<i>w0</i>)	parallel, non-interlaced	0.0625 (15 amu/nm^3)	20 m_0
Weave I (<i>wI</i>)	orthogonal (non interlaced)	0.1875 (45 amu/nm^3)	20 m_0
Weave II (<i>wII</i>)	orthogonal (non interlaced)	0.33 (80 amu/nm^3)	15 m_0
Weave III (<i>wIII</i>)	alternating interlaced	0.35 (84 amu/nm^3)	21 and 17 m_0

Table 1: Density of the different weaves shown in Figure 1

Entanglement of the Polymer Chains

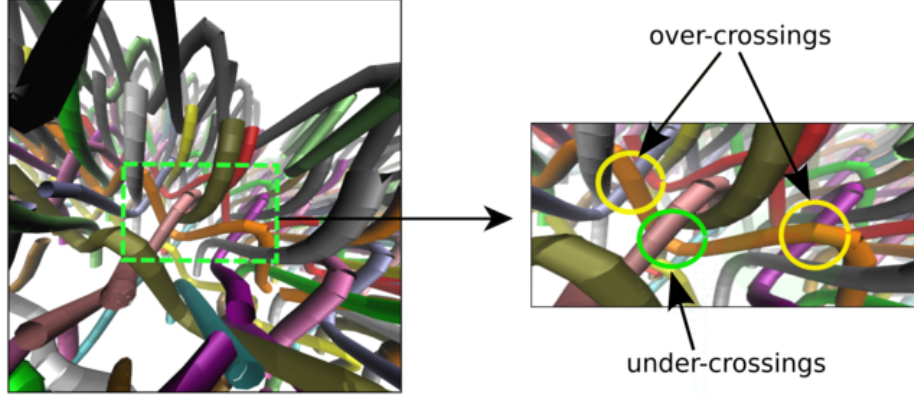


Figure 2: Projection of chains of weaveIII. WeaveIII is an alternating interlaced weave. For example, the chains in the x direction, alternately go over and under chains in the y perpendicular direction, as shown for the orange curve and three chains it meets in a perpendicular direction.

4 Dynamic Model for Polymeric Materials and Computational Methods

We consider entangled macromolecules that we simulate using LAMMPS [49] (<http://lammmps.sandia.gov>). The polymers are treated as elastic macromolecules modeled with harmonic bond potential of energy $E = K_b(r - r_0)^2$, $K_b = 250$, r denotes the length of extension of the polymer bonds and $r_0 = 1$ denotes the rest length of the bond. The polymer bending stiffness is controlled with a harmonic angle potential with energy $E = K_\theta(1 - \cos(\theta - \theta_0))$, with $K_\theta = 8$, where θ is the angle between two consecutive bonds. The rest angle is $\theta_0 = \pi$. With this choice of K_θ , the chains have persistence length approximately $1/5$ of the length of the simulation box. With these potentials, there is no maximum permitted length or bond angle constraints, but there is a high energy penalty for large deviations from the rest length. This does not exclude the possibility of chains crossing through each other, especially for large deformations. Our results however, show that chain crossings are rare enough so as to not influence the qualitative effects of entanglement observed here (see Section 5). Therefore, our systems simulate stiff macromolecules which do not cross each other. We use the Lennard-Jones potential with energy

$$E = 4\epsilon \left(\left(\frac{\sigma}{r} \right)^{12} - \left(\frac{\sigma}{r} \right)^6 \right) \quad (5)$$

with cutoff 2.5σ using Lennard Jones units.

The dynamics are simulated throughout using the Langevin Thermostat:

$$m \frac{dV}{dt} = -\gamma V - \nabla \Phi(X) + \sqrt{2k_B T \gamma} \frac{dB_t}{dt}, \quad (6)$$

where X denotes the position of the atoms, $V = \frac{dX}{dt}$ is the velocity, $-\nabla \Phi(X)$ denotes the force acting on the atoms due to interaction potentials, γ is the friction coefficient and $\sqrt{2k_B T \gamma} dB_t/dt$ is

the random force.

To study the mechanics of the polymeric fluid, we investigate the response of the material to oscillatory shear stress (Lees-Edwards boundary conditions [33]) applied with rate $\dot{\gamma} = \dot{\gamma}_0 \cos(\omega t)$. We place the specimen in minor, sinusoidal oscillation by changing the specified box length to $L(t) = L_0 + A \sin(2\pi \frac{t}{T_p})$.

As a measure of material response, we consider the dynamic complex modulus $G(\omega) = G_1(\omega) + iG_2(\omega)$. The components are defined from measurements of the stress as the least-squares fit of the periodic stress component σ_{xy} by the function $g(t) = G_1(\omega)\gamma_0 \cos(\omega t) + G_2(\omega)\gamma_0 \sin(\omega t)$. This offers a characterization of the response of the material to oscillating applied shear stresses and strains as the frequency ω is varied. The G_1 is referred as the Elastic Storage Modulus and G_2 is described as the Viscous Loss Modulus. These dynamic moduli are motivated by considering the linear response of the stress components σ_{xy} to applied stresses and strains. At low frequency the polymer stresses appear to have sufficient time to equilibrate to the applied shear stresses. At high frequencies, the polymer stresses do not appear to have sufficient time to equilibrate to the applied shear stresses. This is manifested in $\sigma_{xy}(t)$ which is seen to track very closely the applied stress. A phase lag 0 is representative of solids and $\pi/2$ is representative of liquids. This delay is caused by propagating the stress through the domain via the chain topology. The increase of G_2 indicates that the mechanics arises effectively from chains' resistance to more rapid motions, such as sliding, while the increase of G_1 indicates in the mechanics a resistance to direct deformation represented by increases in the elastic bond lengths or from the bending stiffness of chains.

To estimate the dynamic complex modulus in practice, the least-squares fit is performed for $\sigma_{xy}(t)$ over the entire stochastic trajectory of the simulation (after some transient period). In our simulations, the maximum strain over each period was chosen to be half the periodic unit cell in the x -direction, corresponding to a strain amplitude $\gamma_0 = \frac{1}{2}$. A description of the parameters and specific values used in the simulations can be found in Tables 2 and 3.

The effective stress tensor associated with the polymers at a given time is estimated using the Irving-Kirkwood method [12, 26]

$$\sigma_{l,k} = \frac{1}{V} \sum_n \sum_{j=1}^{n-1} \left\langle f_j^{(l)} \cdot (x_{q_n}^{(k)} - x_{q_j}^{(k)}) \right\rangle \quad (7)$$

where V is the volume of the periodic box, $x_{q_v}^{(k)}$ is the k -th coordinate of the q_v -th atom (the minimum image convention is used for the difference) and $f_j^{(l)}$ is the l -th coordinate of the pairwise interaction between the two atoms.

Parameter	Description	Value
σ	monomer radius	1.0 nm
ϵ	energy scale	$2.5 \text{ amu} \cdot \text{nm}^2/\text{ps}^2$
m_0	reference mass	1 amu
w_c	energy potential width	2.5σ
m	monomer mass	$240 m_0$
τ	LJ-time-scale	$\sigma\sqrt{m_0/\epsilon} = 0.6 \text{ ps}$
$k_B T$	thermal energy	1.0 ϵ
ρ	solvent mass density	$39 m_0/\sigma^3$
μ	solvent viscosity	$25 m_0/\tau\sigma$
Υ	drag coefficient	$476 m_0/\tau$

Table 2: *Parameterization for the polymer weave models.*

Parameter	Description	Value
E_b	harmonic bonds potential constant	$619.5 \text{ amu}/\text{ps}^2$
b	harmonic bonds rest length	1.0 nm
E_θ	harmonic angle potential constant	$19.8 \text{ amu} \cdot \text{nm}^2/\text{ps}^2$
θ_0	harmonic angles' rest length	180°

Table 3: *Parameterization for the stiffness and connectivity of the polymer chains.*

Table 4 shows how the simulation time and oscillation period range compare to characteristic times in our systems. We use as a reference time τ_R for an ideal chain of length 20.

Parameter	Description	value
τ_A advection time	propagation in fluid	0.0013 ps
τ_D diffusion time	monomer moves a dist. σ	302 ps
τ_R Rouse time	ideal chain $N = 20$	6937 ps
τ_0 critical time	cross-over reference time	598 ps
T	period of oscillation	$6\text{ps} < T < 3600\text{ps}$
t simulation time	timescale of longest simulation	$150\text{ps} < t < 90000\text{ps}$

Table 4: *Characteristic time scales*

5 Bulk Mechanical Responses of the Polymeric Materials

5.1 Complex modulus

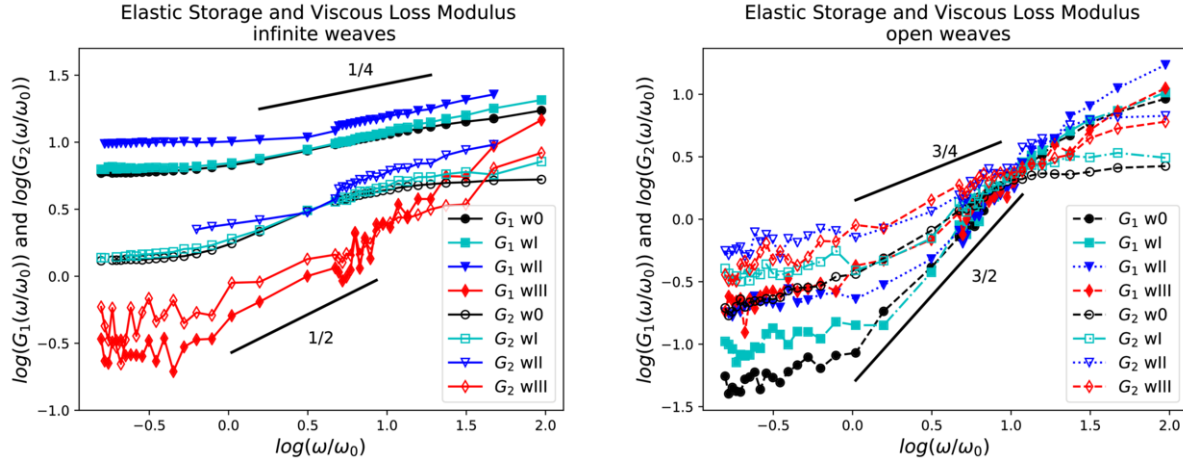


Figure 3: *Polymer Weave Frequency Response: Dynamic Moduli.* The Elastic Storage and Viscous Loss Moduli of the infinite chain weaves are shown on the left and those of the open chain weaves on the right. The infinite weaves behave like crosslinked polymers with a primarily elastic behavior throughout the range of frequencies simulated. The exponents 1/2 and 1/4 are similar to those in the Rouse model [15]. The open weaves transition from an elastic to a viscous behavior as frequency is varied. The exponents 3/4 and 3/2 indicate the predicted scaling for semi-dilute solutions of semi-flexible chains and for the BEL model respectively [15]. The slope increases with decreasing topological complexity.

We show the log-log plot of the Elastic Storage Modulus G_1 and Viscous Loss Modulus G_2 for all the infinite and open weave polymeric materials as the shear response frequency is varied in Figure 3. The frequency of oscillation is normalized by $\omega_0 = 2\pi/\tau_0$ where $\tau_0 = 943\tau = 598ps = 1.98\tau_D$ is a time-scale on the order of the diffusion time τ_D (see Table 4).

Comparing G_1, G_2 for the infinite weaves we see that, in the range of frequencies studied, we have $G_1 > G_2$ for all the simple weaves. The crossover of G_1 and G_2 is absent for those systems within this range of frequencies, which indicates no behavioral transition in the samples which exhibit solid properties. When G_1 is larger than G_2 the elastic response is dominant indicating there is relatively few polymer rearrangements (reptation) within the network structure. This indicates that energy is mainly stored elastically in the stretching and bending of bridging polymeric chains. This can be verified by our *Writhe* quantity for the chains as it reaches a minimum at the extrema of the oscillatory strain period within this regime (see Section 5.2).

The systems with large G_1 behave like stiff materials having strong entanglements similar to imperfect networks having transient covalent crosslinking [9, 25, 34, 41, 51, 52, 61]. This indicates that polymer solutions of long linear semiflexible chains can behave like crosslinked networks, even in the absence of explicit crosslinks. This feature could be useful in understanding some of the viscoelastic properties exhibited by collections of microtubules and the responses of the cytoskeleton [36].

Initially, G_1 and G_2 are independent of the frequency of oscillation and we see a crossover at frequency ω_0 that corresponds to period τ_0 . At frequencies higher than ω_0 (period times shorter

than τ_0) there is a significant dependence of moduli on the frequency which increases with increasing topological complexity. This is in agreement with predictions for polymeric networks [15]. The line segments shown in the figure indicate a scaling between $\sim \omega^{1/4}$ and $\sim \omega^{1/2}$, respectively, to be compared with that of Rouse chains.

The alternate interlacing weave, wIII, is the only infinite weave for which G_1, G_2 intersect and for which G_1 and G_2 both seem to scale as $\omega^{1/2}$ in the intermediate frequencies. Moreover, for wIII, $G_1 \approx G_2$, with $G_1 < G_2$ for low frequencies. We find that the original configuration of wIII is not favorable to the stiffness of the chains and the chains need to stretch resulting in a larger G_1 . This causes extra collisions with other chains which results in larger values of G_2 as well.

Comparing G_1, G_2 for the open systems we find that both G_1 and G_2 are initially constant up to $\omega \approx \omega_0$ and then increase and intersect at $\omega \approx 10\omega_0$. We have $G_2 < G_1$ for $\omega < 10\omega_0$ and $G_1 < G_2$ for $\omega > 10\omega_0$. This suggests two critical times in the polymer chain dynamics. The first is $\tau_e = \tau_0/10$ and the second is τ_0 at which we find have a trend of slightly increasing with decreasing density of the systems as predicted in [38]. We find that with increasing frequency the response tends to become dissipative.

At low frequencies $G_1 \sim \omega^{1/2}$ we find the trends follow the Rouse model. For larger frequencies we find that $G_1 \sim \omega^{3/2}$, $G_2 \sim \omega^{3/4}$ and then G_1, G_2 tend to a plateau value. Similar scalings were reported in [65]. We remark that the empirical model of Barlow et al (BEL model, [6]) predicts $G_1 \sim \omega^{3/2}$ at low frequencies for low molecular weight liquids and $G_2 \approx \omega^{3/4}$ corresponds to the terminal response of semiflexible unentangled chains, similar to semidilute solutions of actin and tubulin [8]. Similar behaviors have also been observed in the transition region between the plateau and the glassy region of linear polymer melts of high molecular weight [48]. We find a decreasing slope of G_1 for increasing entanglement which suggests a slower relaxation mechanism. Considering the complex modulus as an effective sum of that for low molecular weight liquids and the Rouse model, these results indicate there is an effective Rouse mode for the alternating weave wIII polymeric material and for the dense orthogonal weave wII material, but none for the simple weave materials w0 and wI. This suggests that there exists a threshold level of entanglement for the Rouse model to apply. Similar findings have also been reported in [10, 40, 63, 66].

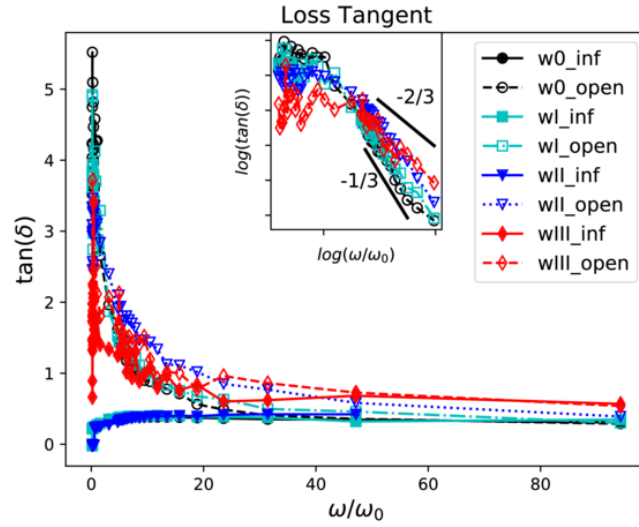


Figure 4: Polymer Weave Frequency Response: Loss Tangent. The infinite systems behave like crosslinked polymers with a loss tangent less than 1 at all frequencies. The open chains transition from a liquid-like behavior to that of a solid-like behavior as the frequency increases. The inset plot shows the log-log plot for open chains. These results show that the crossover frequency increases with decreasing topological complexity. Similarly, the slope of decrease increases with decreasing topological complexity.

We show the loss tangent as a function of the frequency of oscillation in Figure 4. We remark that $\tan \delta$ can be interpreted as reflecting the strength of what is sometimes called “colloidal forces”. In other words, if $\tan \delta < 1$ then the particles are highly associated and sedimentation could occur. If $\tan \delta > 1$, the particles are highly unassociated. The loss tangent is almost constant, close to 0, for all the simple infinite weaves ($w0, wI, wII$). The values of the open weaves are greater than one and then decrease to the values of the corresponding infinite weaves. The asymptotic ordering of the phase lag of the systems is $w0 < wI < wII < wIII$. We find that, our data at larger frequencies that all the materials behave like elastic solids, as is often seen in large frequency responses. The inset graph shows the corresponding log-log plot only for the open systems. It reveals a cross-over at approximately ω_0 , which corresponds to times on the order τ_0 . This time-scale could be related to the entanglement time as in [16, 60]. This characteristic time-scale, seems to decrease with the topological complexity of the weave. The large frequency tail of $\tan \delta$ decreases more slowly with increasing topological complexity and density indicating a substantial dissipation effect related to entanglement.

5.2 Conformational analysis

We show configurations of the polymer weaves at different times during deformation in Figures 5, 6, 7, 8. For the small oscillation frequencies, the infinite chains follow the deformation of the defining box, attaining an s-shape conformation. The open chains, significantly rearrange in time and tend to avoid the boundary by aligning with the orientation of the deformation. This process happens more slowly for wI and even more slowly for wII and $wIII$ systems due to topological obstacles. We note that the chains tend to form bundles of chains, giving an inhomogeneous material, suggesting

that the inhomogeneity decreases with increasing density and entanglement complexity. Similar phase separation of polymer solutions in oscillatory shear has been observed experimentally in [55]. We find the transition from bundle-dominated structures to entanglement dominated structures is related to the entanglement length of the chains as has been also reported in [57]. The chains bundle together in order to decrease their deformation. As the chains bundle, they form tubes of chains. A larger diameter tube resists the deformation stronger than the individual chains. This larger tube structure is apparent in the w0 infinite system. The same happens in two and three directions respectively for wI, wII and wIII. This also happens transiently at initial times for the open systems. At first the open chains form these bundles then they keep rearranging and entangling further until finally forming globules.

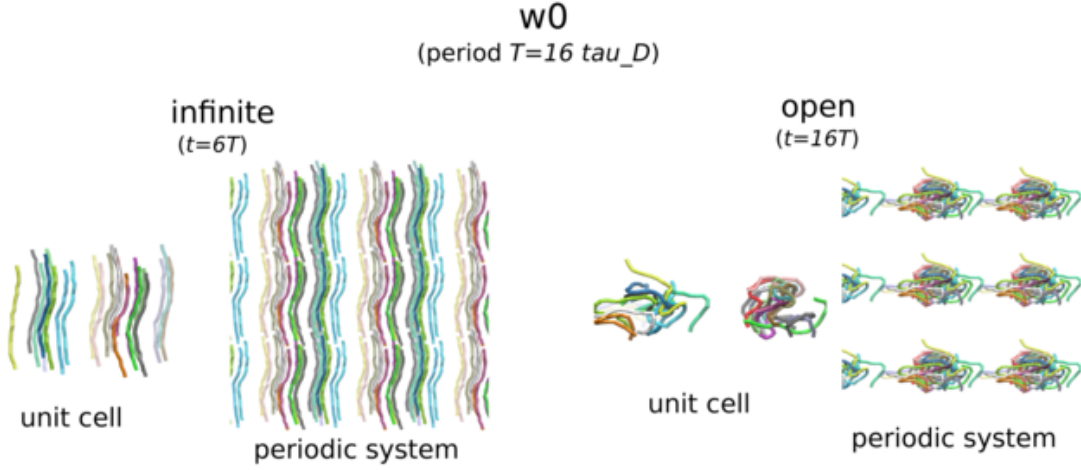


Figure 5: Polymer *weave0* subject to oscillatory shear. Configurations at the end of the simulation for the infinite and corresponding open system. In both cases, the chains tend to form bundles. By forming tubes of larger radius the chains decrease their individual deformation. The open chains can significantly rearrange their conformations to those of random coils and the system becomes inhomogeneous, disconnected across the periodic boundary.

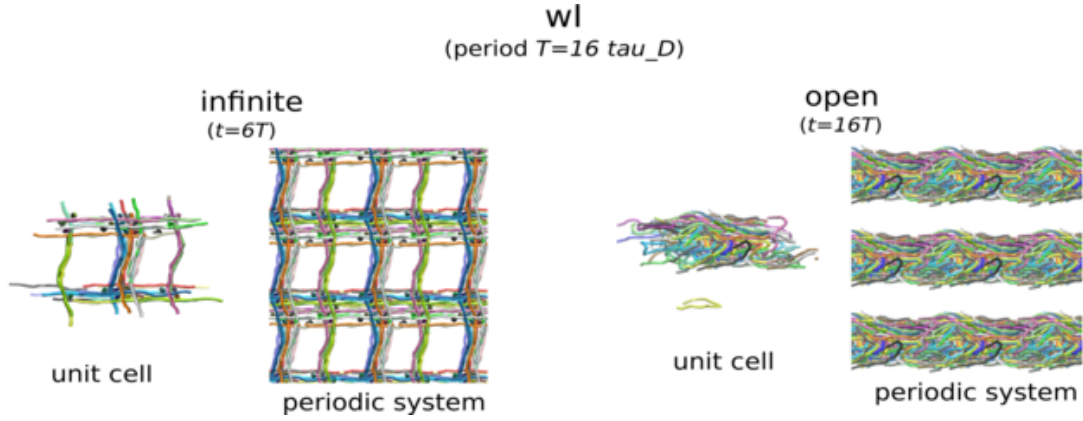


Figure 6: Polymer weaveI subject to oscillatory shear. Configurations at the end of the simulation for the infinite and corresponding open system. In both cases, the chains tend to form bundles. The open chains can significantly rearrange their conformations, forming lamellar structures in one direction. The reason for the tube and lamellar formations in the infinite and open chains, respectively, is that this reduces the individual deformation of the chains.

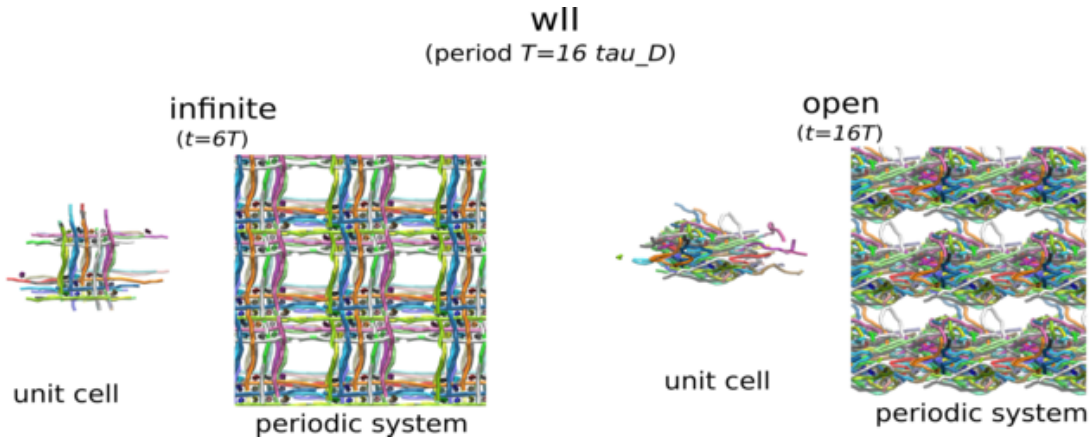


Figure 7: Polymer weaveII subject to oscillatory shear. Configurations at the end of the simulation for the infinite and corresponding open system. In both cases, the chains tend to form bundles to reduce their individual deformation. The open chains can significantly rearrange their conformations to form lamellar structures in one direction which tend to become 2 dimensional.

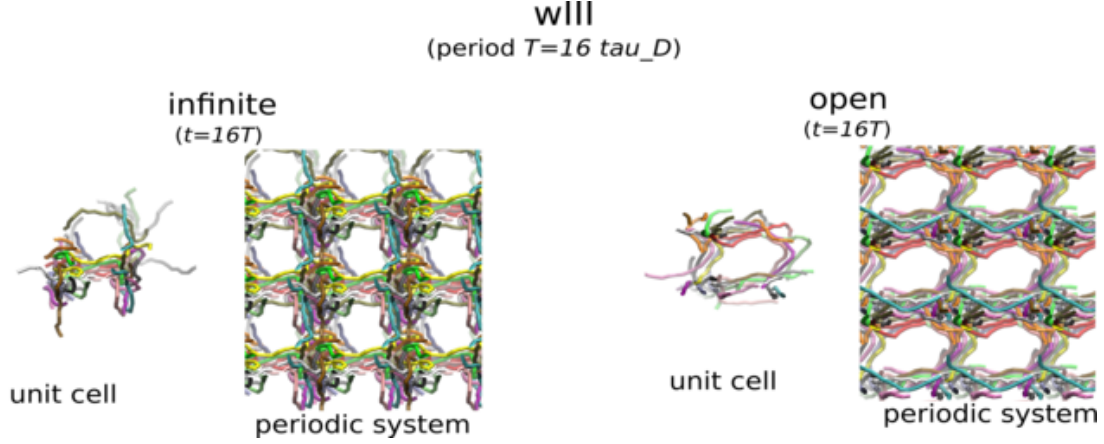


Figure 8: Polymer weaveIII subject to oscillatory shear. Configurations at the end of the simulation for the infinite and corresponding open system. In both cases, the chains tend to form bundles to reduce their individual deformation. The open chains are trapped by entanglements, resembling the corresponding infinite weave. The open system retains the percolation of entanglement in 3 dimensions.

Our topological methods can be used to more precisely characterize the conformational features of the chains. We do this by measuring the *Writhe* and the *Periodic Linking Number* topological quantities that we introduced in Section 2. We remark that the chains in our system are loosely entangled relative to highly knotted systems yielding, as a consequence, Periodic Linking Numbers and Writhe that are less than one. While the quantities appear small relative to those of highly knotted systems, they still provide a useful characterization of the collective configurations of the polymeric chains of the material and their rearrangements. As our results indicate these are useful in understanding the connection between topology and mechanical responses.

We show the time evolution of the Writhe for the weave of type w0 for the fixed frequency of oscillation, $T = 12\tau_D$ in the cases of infinite and open systems in Figure 9. We find a very different behavior between the open and infinite systems (the situation is similar for wI and wII). In the case of the infinite periodic systems, the mean absolute Writhe of the chains shows a sinusoidal behavior. This is seen most clearly when the frequency of oscillation is small. This reaches a minimum and a maximum each $\delta t = T/4$. During the shearing cycle of the unit cell in our simulations, the Writhe is maximum when the shear deformation is the least and the Writhe reaches a minimum when the shear deformation is at its greatest. This behavior is indicative of the chains stretching at the maximum deformation and relaxing to a more entangled state when the shear deformation is relaxed.

The formation of bundles causes a small decay of Writhe over time. This manifests once the chains have formed bundles with their Writhe following a sinusoidal behavior with a lower average amplitude. In the case of open systems, the mean absolute Writhe of the chains also follows a sinusoidal behavior, but it changes significantly in time. This happens because the chains are free to attain any possible configuration and tend to disentangle and relax to configurations similar to those of random coils. Indeed, the final values are similar to those of a semiflexible random coil of comparable length as reported in [46]. This behavior becomes less pronounced as we increase the density and complexity of the weave because the disentanglement time increases and the chains do not have sufficient time to rearrange. Indeed, in the case of wIII, the Writhe of the open chains does not vary significantly, behaving similarly to the infinite chains, indicating that the chains are

constrained by entanglements (see Figure 9). We also notice that, for w_{III} , the Writhe of the open chains is smaller than that of the infinite chains. A reason for this appears to be that the chains attain more stretched and straightened conformations in order to decrease their bending energy in the arrangements inherited from the original chain configurations.

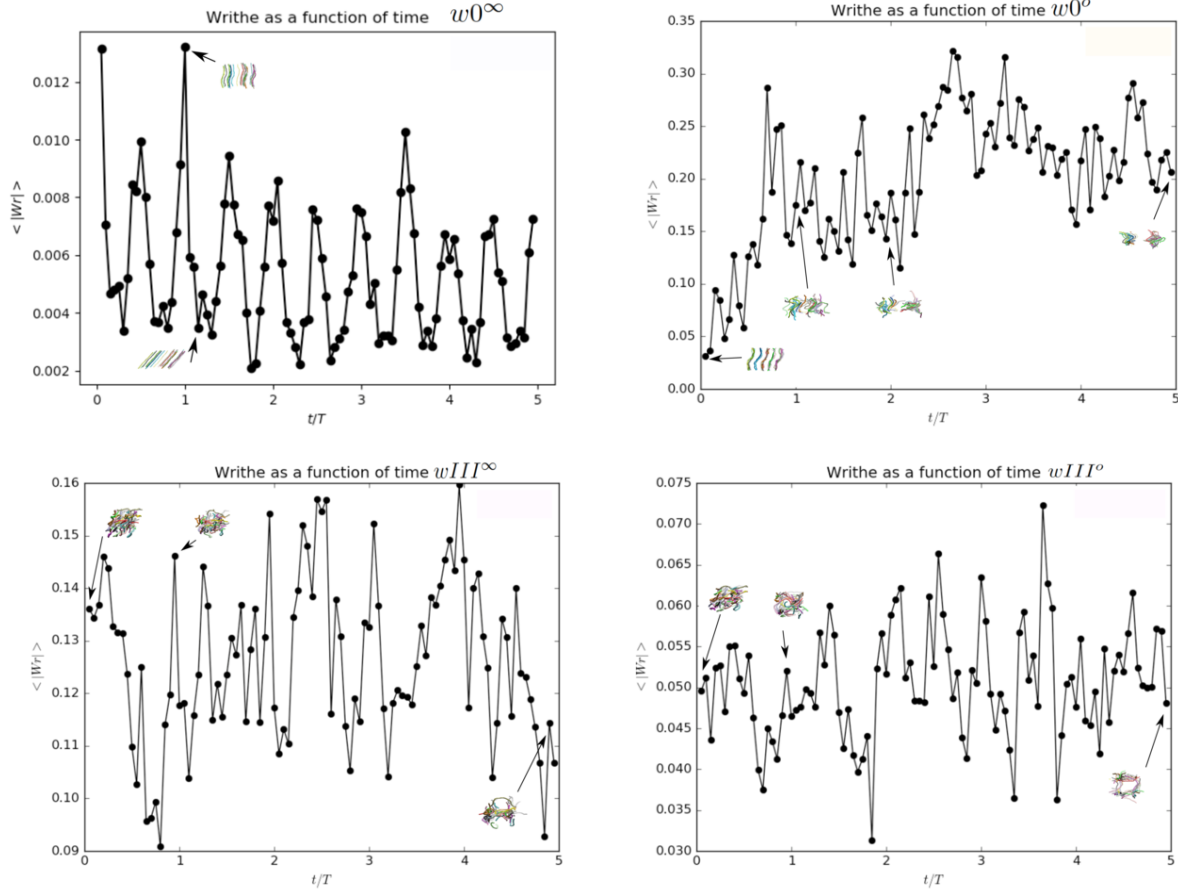


Figure 9: The evolution of the mean absolute Writhe as a function of time during an oscillatory shear experiment. Data shown for w_{weave0} (above) and $w_{weaveIII}$ (below) for period of oscillation $T = 12\tau_D$, for total time $5T$. Left: infinite weaves, Right: open weaves. The Writhe is a fingerprint of the motion of the chains. The infinite chains stretch and relax according to the shear motion of the cell. The open chains re-arrange their conformation to reduce the stress. The behavior is different for w_0 and w_{III} . In the absence of constraints, the chains behave like random coils increasing their Writhe. In the presence of constraints, the chains relax at conformations that reduce their bending and, therefore, their Writhe, in order to escape entanglements.

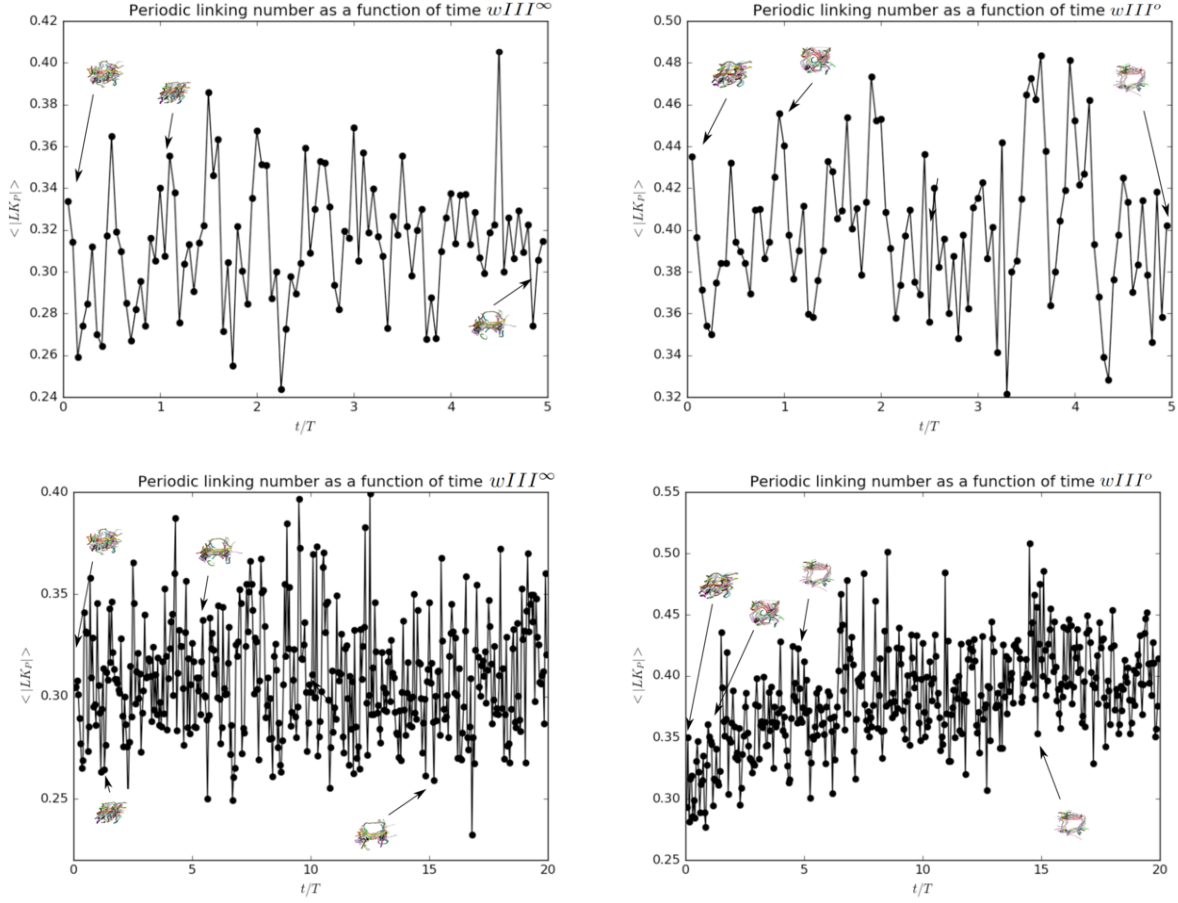


Figure 10: The evolution of the mean absolute Periodic Linking Number as a function of time during an oscillatory shear experiment. Data shown for weaveIII for period of oscillation: Above: $T = 12\tau_D$, for total time $5T$, Below: for period $T = 6\tau_D$, for total time $20T$. Left: infinite weave, Right: open weave. The absence of an abrupt change in the data is indicative of no chain crossings, even at high frequencies. The Periodic Linking Number of the infinite chains fluctuates around a value. The Periodic Linking Number of the open chains increases, indicating that the chains create stronger contacts as they try to escape their original constraints, similar to what was observed for linear FENE chains in a melt under elongation in [45].

The presence of topological constraints in weave wIII is also supported by our results concerning the Periodic Linking Number. We show the time evolution of the mean absolute Periodic Linking Number for a fixed frequency of oscillation, $T = 12\tau_D$, for weave wIII in Figure 10. We see that the values of the Periodic Linking Number are similar for infinite and open wIII systems, confirming that in these time scales the entanglement dominates. These results also show that any chain crossing that might occur due to the use of the harmonic bond potential is not significant (or even absent).

To further examine the latter, we analyze the the Periodic Linking Number of wIII chains, both infinite and open, at a higher frequency of oscillation, $T = 6\tau_D$, and for a longer time, $t = 20T$, see Figure 10. We note that the Periodic Linking Number does not show a trend that would imply a significant disentanglement due to chain crossings. For open chains, we see that the mean absolute

Periodic Linking Number initially increases. A reason for this appears to be that as the chains tend to straighten out to reduce their bending energy they also tighten up their contacts with the other nearby chains. This results in an increase in the effective chain-chain linking. A similar behavior for the linking number was observed for polymer melts of linear FENE chains in an elongational flow in [45]. In view of these facts, we believe that the effect of the use of the harmonic bonds does not alter the qualitative analysis of our data.

5.3 Topology and Mechanical Responses

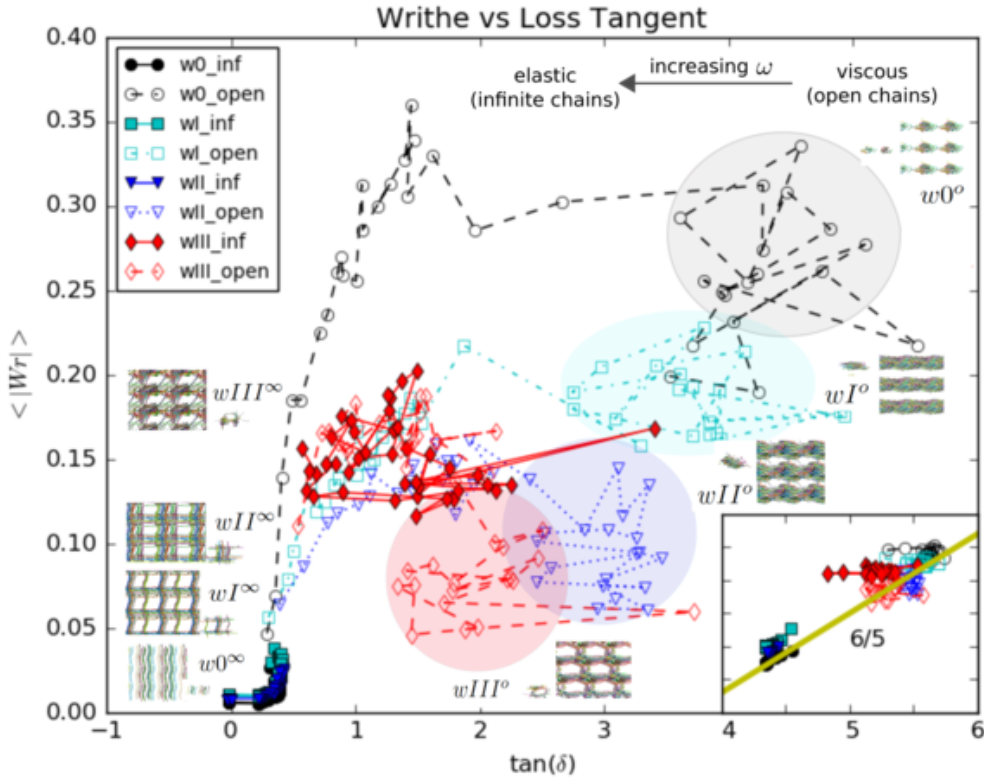


Figure 11: Writhe and Loss Tangent. We find a linear behavior of the Writhe as a function of the Loss Tangent. The data points corresponding to the different weaves form clusters. For open chains as the topological complexity of the weave decreases both the Writhe and Loss Tangent increase. As the oscillation frequency increases, the chains transition to the values of corresponding infinite weaves. The infinite weaves $w0$, wI and wII have very similar Writhe, indicating steady-state similar collective configurations of the polymer chains. The inset plot shows the log-log plot of small frequency responses which have characteristic scaling $\langle |Wr| \rangle \sim (\tan \delta)^{6/5}$.

We show the mean absolute Writhe of the chains as a function of the loss tangent in Figure 11. We find a decay of the mean absolute Writhe with the loss tangent and a clustering of the data for each system. We see that, as the frequency increases, the Writhe of the open systems tend to

meet the values of their corresponding infinite chain versions. This occurs since the chains cannot escape their original configuration as readily at large oscillation frequencies. The infinite systems of similarly almost trivial topology show the same response to deformation and only the weave with higher topological complexity (threading) gives a different response. It is notable that the proposed Writhe measure groups together the systems of similar material response.

The inset of Figure 11 shows a log-log plot of responses for small frequencies of oscillation. These results show a relationship between Writhe and $\tan \delta$ that scales like $\langle |Wr| \rangle \sim \tan \delta^{6/5}$. The responses at small frequencies are clustered and ordered with their Writhe increasing as: $w0 \approx wI \approx wII < wIII$ for the infinite chains and decreasing as $w0 > wI > wII > wIII$ for the open chains. For the $wIII$ case, approximately the same values for open and infinite chains are found.

For the infinite systems, we observe that the Writhe does not change significantly. This is expected, since without breakage of bonds the topology must remain close to that of the original configuration. Since $w0, wI$ and wII start with individually straight chains, their Writhe remains close to 0. The original configuration of $wIII$ has larger individual Writhe values and remains at the level 0.15. This is another indication that there is no change in chain entanglement.

For the open chains, there is the potential for significant rearrangements of polymer chain configurations and topology. The open chains tend to attain configurations similar to those of random coils of comparable stiffness. However, attaining this state is significantly obstructed by entanglements. This results in a decrease of the Writhe with entanglement complexity and density. The clustering observed for these systems indicates that the global entanglement of the chains imposed by the original conformation affects the response of the material significantly. The clustering shows that these distinct behaviors arising from topology can be characterized by our mean absolute Writhe of the chains.

Previous studies have shown that there is almost a linear relationship between the number of kinks per chain and the mean absolute Writhe of a chain in a melt in the case of linear FENE chains as a function of molecular weight in equilibrium conditions [46]. In non-equilibrium conditions however, the relation becomes more complex [45]. The viscosity, can be obtained as the limit $\eta = \lim_{\omega \rightarrow 0} G_2(\omega)/\omega$. Our results for the smallest frequencies indicate that the Writhe of the open chains decreases with G_2/ω , suggesting a decrease of the Writhe with viscosity, see Figure 12. The number of kinks has been shown to increase with viscosity [5, 28]. A similar inverse behavior between the Writhe of the chains and the number of kinks was observed in the initial times of elongation of the chains [45].

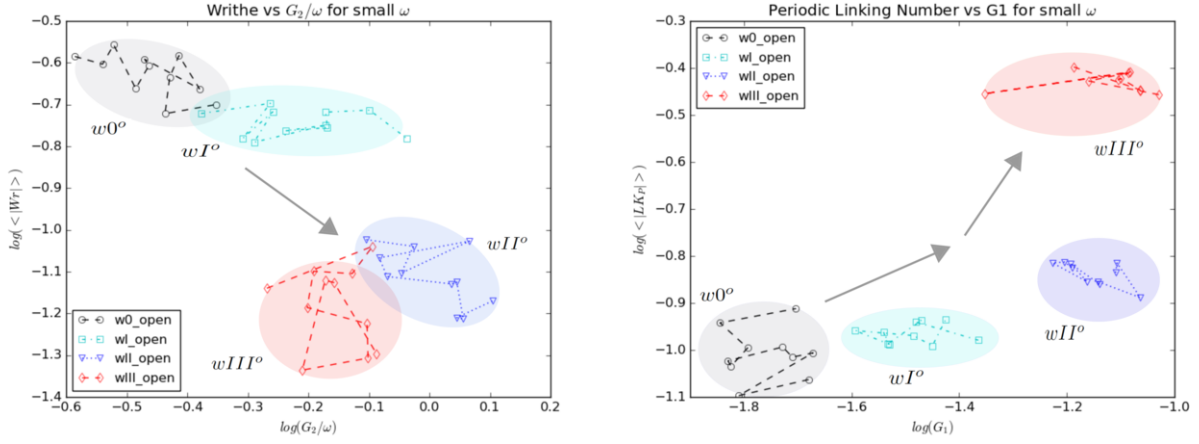


Figure 12: Left: Writhe and G_2/ω for open weaves at small frequencies (log-log plot). The viscosity can be obtained as the limit $\eta = \lim_{\omega \rightarrow 0} G_2(\omega)/\omega$. We find an indication that the Writhe decreases with viscosity, while Z shows the opposite relation to viscosity [5]. Right: Periodic Linking Number as a function of G_1 for open chains for small frequencies (log-log plot). The equilibrium modulus can be obtained as the limit $G_{eq} = \lim_{\omega \rightarrow 0} G_1(\omega)$. We find an indication that G_{eq} increases with increasing linking, similar to what was reported for rings in [19].

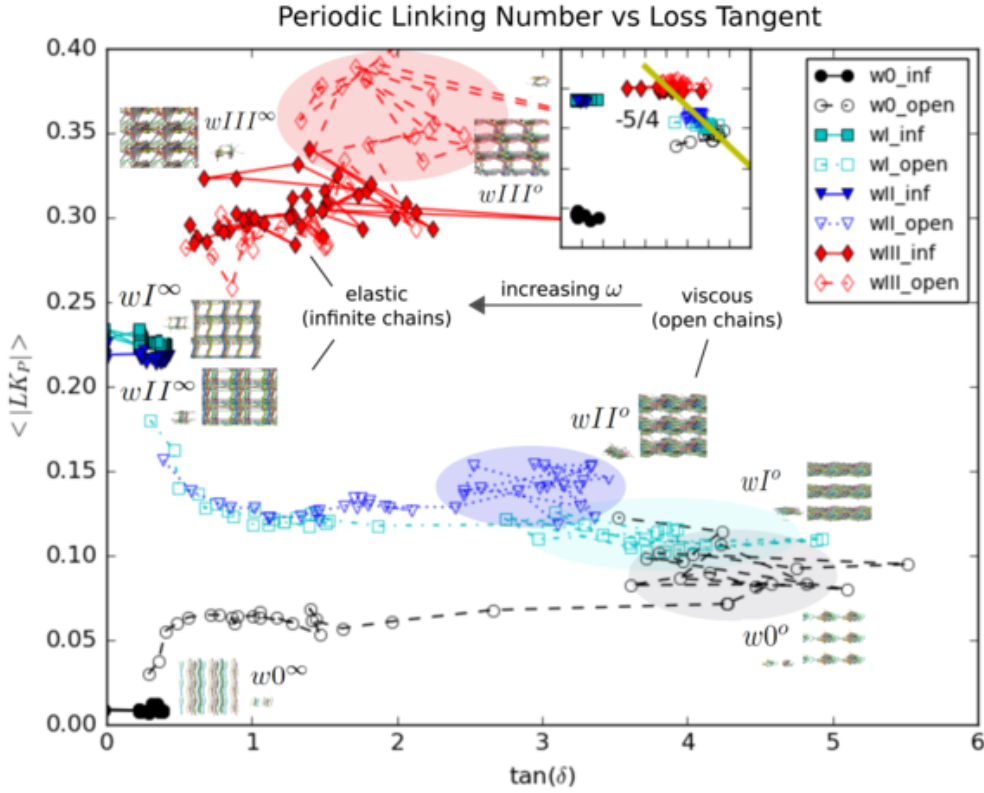


Figure 13: Periodic Linking Number and Loss Tangent. We find that the responses corresponding to the different weaves form clusters. The Periodic Linking Number of the open chains increases with weave complexity and decreases with loss tangent. As the frequency increases the open chain values transition to those of the corresponding infinite weave. The linking numbers of weaves wI and II are very similar indicating similar behaviors. The inset plot shows the log-log plot of small frequency responses which have characteristic scaling $\langle |LK_P| \rangle \sim (\tan \delta)^{-5/4}$.

We show the mean absolute Periodic Linking Number as a function of the loss tangent in Figure 13. We find that the mean absolute Periodic Linking Number decreases with the loss tangent for $\tan \delta > 1$. We find significant clustering of the data corresponding to the different systems. With increasing frequency, the open systems tend to the value of the corresponding infinite systems. This occurs because, at large frequencies, the open chains cannot escape their original configurations.

The inset graph shows the corresponding log-log plot for the smallest frequencies. For $\tan \delta > 1$ the responses are fitted to a relation of the form $\langle |LK_P| \rangle \sim \tan \delta^{-5/4}$. The increase of the linking number implies the presence of persistent entanglements. Persistent entanglements are tight contacts between chains that significantly restrict their motion [1]. Such contacts are likely to cause significant bond stretching under deformation that is followed by a decrease of the Loss Tangent. The clustering of the responses indicates that the imposed global topology of the initial configuration affects significantly the response of the material. This persists for long durations even in the cases we considered, in which the topology is allowed to change over time. These results show that interactions underlying mechanical responses can be effectively captured by the Periodic Linking Number.

From our results we obtain information about the equilibrium modulus. The equilibrium modulus is defined as the limit $G_{eq} = \lim_{\omega \rightarrow 0} G_1(\omega)$. We show the storage modulus for the smallest frequencies in Figure 12. Our results suggest that the equilibrium modulus increases with the linking of the chains. Interestingly, a similar linear relation between the entanglement density as obtained from the Gauss linking integral and the shear modulus for ring polymers was reported in [19].

Our results on the Writhe and Periodic Linking Number show a competing relation between these two with respect to the Loss Tangent. We provide a brief explanation for this effect in the case of open chains. If the Writhe is large and the Periodic Linking Number is small, this can be interpreted as meaning the chains attain random conformations with no significant topological constraints. This would result in a behavior that is primarily dissipative. This suggests that interchain contributions to stress dominate through collisions of molecules induced by Brownian motion.

In contrast when the Writhe is small and the Periodic Linking Number is large, we expect that the chains get stretched by the presence of persistent entanglements. In this case, intrachain contributions to stress would dominate. As the ratio $\langle |LK_P| \rangle / \langle |Wr| \rangle$ increases, the persistence of entanglements increases. This implies that the bond stretching increases, which decreases the Loss Tangent. Therefore, we expect the loss tangent to increase with such decreasing ratio of Periodic Linking Number versus Writhe. In fact, this is confirmed in our results as seen in Figure 14. Our results show, for the open systems at small frequencies, such a trend of the ratio of the Periodic Linking Number over the Writhe as a function of the Loss Tangent. This indicates that one can control the viscoelastic properties of a material by controlling the ratio of the Writhe and Periodic Linking Numbers of the constituent chains. This also suggests that $\langle |LK_P| \rangle / \langle |Wr| \rangle$ is a measure of the interchain contribution versus the intrachain contribution to the stress, a finding that may contribute to our understanding of the interplay between these two contributions [59].

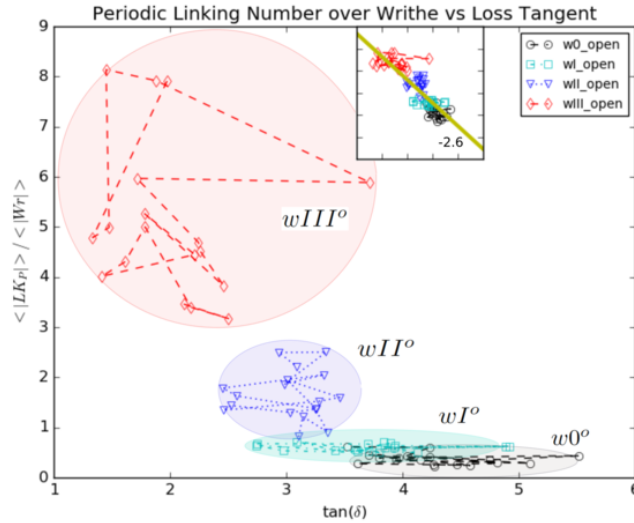


Figure 14: The ratio of the Periodic Linking Number over the Writhe as a function of the loss tangent for open systems at low frequencies (inset: double logarithmic plot). We notice that the ratio $\langle |LK_P| \rangle / \langle |Wr| \rangle$ decreases with the loss tangent. The inset plot shows the log-log plot of small frequency responses which have characteristic scaling $\langle |LK_P| \rangle / \langle |Wr| \rangle \sim (\tan \delta)^{-2.6}$.

6 Conclusions

We have introduced for polymeric materials topological measures for quantifying the relationship between polymer chain entanglement and viscoelastic responses. We investigated the link between molecular-level interactions and mechanical responses for polymeric materials having weave-like topologies using non-equilibrium molecular dynamics simulations. We found that our proposed measures in conjunction with the mechanical Storage and Loss Moduli resulted in significant clustering distinguishing the different polymeric materials considered. Our results indicate that our topological measures provide a useful quantity for understanding how the molecular-level polymer chain entanglements contribute to aggregate mechanical responses. Our results can be used more generally as topological tools to further develop polymer theories to understand the interplay between entanglement and mechanics. It would be interesting also to explore in future work how our topological measures could be included to improve mean field theories and related formalisms [22,43] and when incorporating additional effects such as hydrodynamic coupling [2–4,64].

7 Acknowledgments

The author P.J.A acknowledges support from research grant NSF CAREER DMS-0956210, NSF DMS - 1616353, and DOE ASCR CM4 DE-SC0009254. We also acknowledge UCSB Center for Scientific Computing NSF MRSEC (DMR-1121053) and UCSB MRL NSF CNS-0960316.

References

- [1] S. Anogiannakis, C. Tzoumanekas, and D. N. Theodorou. Microscopic description of entanglements in polyethylene networks and melts. *Macromolecules*, 45:9475–9492, 2012.
- [2] P. J. Atzberger. Stochastic eulerian lagrangian methods for fluid-structure interactions with thermal fluctuations. *J. Comp. Phys.*, 230:2821–2837, 2011.
- [3] P. J. Atzberger. Incorporating shear into stochastic eulerian-lagrangian methods for rheological studies of complex fluids and soft materials. *Physica D*, 265:57–70, 2013.
- [4] P. J. Atzberger, P. R. Kramer, and C. S. Peskin. A stochastic immersed boundary method for fluid-structure dynamics at microscopic length scales. *J. Comp. Phys.*, 224:1255–1292, 2007.
- [5] C. Baig, V. G. Mavrantzas, and M. Kröger. Flow effects on the melt structure and entanglement network of linear polymer melts: Results from a nonequilibrium molecular dynamics simulation study of a polyethylene melt in steady shear. *Macromolecules*, 43:6996, 2010.
- [6] A. J. Barlow, A. Egrinsav, and J. Lamb. Viscoelastic relaxation in poly-1-butenes of low molecular weight. *Proc. R. Soc. Lond. A*, 300:356–372, 1967.
- [7] W. Bisbee, J. Qin, and S. T. Milner. Finding the tube with isoconfigurational averaging. *Macromolecules*, 44:8972–8980, 2011.
- [8] D. Boal. *Mechanics of the cell*. Cambridge Univ. Press, 2002.

- [9] A. H. Clark and S. B. Ross-Murphy. Structural and mechanical properties of biopolymer gels. *Adv. Poly. Sci.*, 83:57–192, 1987.
- [10] R. H. Colby, L. J. Fetters, and W. W. Grassley. Melt viscosity-molecular weight relationship for linear polymers. *Macromolecules*, 20:2226–2237, 1987.
- [11] P. G. de Gennes. *Scaling concepts in Polymer Physics*. Cornell University Press, 1979.
- [12] M. Doi and S. F. Edwards. *The Theory of Polymer Dynamics*. Clarendon Press, Oxford, 1986.
- [13] F. Edwards. Statistical mechanics with topological constraints: I. *Proc Phys Soc*, 91:513–9, 1967.
- [14] F. Edwards. Statistical mechanics with topological constraints: Ii. *J Phys A: Gen Phys*, 1:15–28, 1968.
- [15] S. F. Edwards, H. Takano, and E. M. Terentjev. Dynamic mechanical response of polymer networks. *J. Chem. Phys.*, 113:5531, 2000.
- [16] S. F. Edwards, H. Takano, and E. M. Terentjev. Dynamic mechanical response of polymer networks. *J. Chem. Phys.*, 113:5531, 2000.
- [17] M. E. Evans, V. Robins, and S. T. Hyde. Periodic entanglement ii: weavings from hyperbolic line patterns. *Acta Chryst.*, A69:262–275, 2013.
- [18] R. Everaers. Topological versus rheological entanglement length in primitive-path analysis protocols, tube models, and slip-link models. *Phys. Rev. E*, 86:022801, 2011.
- [19] R. Everaers and K. Kremer. Topological interactions in model polymer networks. *Phys. Rev. E.*, 53:R37–R40, 1996.
- [20] R. Everaers, S. K. Sukumaran, G. S. Grest, C. Svaneborg, A. Sivasubramanian, and K. Kremer. Rheology and microscopic topology of entangled polymeric liquids. *Science*, 303:823, 2004.
- [21] K. Foteinopoulou, N. C. Karayiannis, M. Laso, M. Kröger, and L. Mansfield. Universal scaling, entanglements and knots of model chain molecules. *Phys. Rev. Lett.*, 101:265702, 2008.
- [22] G. H. Fredrickson. *The equilibrium theory of inhomogeneous polymers*. Oxford University Press, 2013.
- [23] K. F. Gauss. *Werke*. Kgl. Gesellsch. Wiss. Göttingen, 1877.
- [24] R. S. Hoy, K. Foteinopoulou, and M. Kröger. Topological analysis of polymeric melts: Chain-length effects and fast-converging estimators for entanglement length. *Phys. Rev. E*, 80:031803, 2009.
- [25] K. Hyun, S. H. Kim, K. Hyun Ahn, and S. J. Lee. Large amplitude oscillatory shear as a way to classify the complex fluids. *J. Non Newtonian Fluid Mech.*, 107:51–65, 2002.
- [26] J. H. Irving and J. G. Kirkwood. The statistical mechanical theory of transport processes. *J. Chem. Phys.*, 18:817–829, 1950.

- [27] A. Jain, B. Dünweg, and R. Prakash. Dynamic crossover scaling in polymer solutions. *PRL*, 109:088302, 2012.
- [28] J. M. Kim, D. J. Keffer, B. J. Edwards, and M. Kröger. Rheological and entanglement characteristics of linear-chain polyethylene liquids in planar cuette and planar elongational flow. *J. Non-Newtonian Fluid Mech.*, 152:168–183, 2008.
- [29] K. Kremer and G. S. Grest. Dynamics of entangled linear polymer melts: A molecular-dynamics simulation. *J. Chem. Phys.*, 92:5057–5086, 1990.
- [30] M. Kröger. Shortest multiple disconnected path for the analysis of entanglements in two- and three-dimensional polymeric systems. *Comput. Phys. Commun.*, 168:209–232, 2005.
- [31] M. Kröger, J. Ramirez, and H. C. Öttinger. Projection from an atomistic chain contour to its primitive path. *Polymer*, 43:477–487, 2002.
- [32] S. Kuei, A. M. Slowicka, M. L. Ekiel-Jezewska, E. Wajnryb, and H. A. Stone. Dynamics and topology of a flexible chain: knots in steady shear flow. *New J. Phys.*, 17:053009, 2015.
- [33] A. W. Lees and S. Edwards. The computer study of transport processes under extreme conditions. *J. Phys. C: Solid state phys.*, 5:1921, 1972.
- [34] C. Lieu, R. Durairaj, and S. Ramesh. Rheological studies of pmma-pvc based polymer blend electrolytes with litfsi as doping salt. *PLOS*, 9:e102815, 2014.
- [35] A. E. Likhtman and T. C. B. McLeish. Quantitative theory for linear dynamics of linear entangled polymers. *Macromolecules*, 35:6332–6343, 2002.
- [36] Y. Lin, G. H. Koenderink, F. C. MacKintosh, and D. A. Weitz. Viscoelastic properties of microtubule networks. *Macromolecules*, 40:7714–7720, 2007.
- [37] C. Liu, J. He, E. Ruymbeke, R. Keunings, and C. Bailly. Evaluation of different methods for the determination of the plateau modulus and the entanglement molecular weight. *Polymer*, 47:4461–4479, 2006.
- [38] T. G. Mason, A. Dhople, and D. Wirtz. Linear viscoelastic moduli of concentrated dna solutions. *Macromolecules*, 31:3600–3603, 1998.
- [39] K. C. Millett, A. Dobay, and A. Stasiak. Linear random knots and their scaling behavior. *Macromolecules*, 38:601–606, 2005.
- [40] N. J. Mills and A. Nevin. Oscillatory shear measurements on polystyrene melts in the terminal region. *J. Pol. Sci.*, 9:267–281, 1971.
- [41] S. A. Mortazavi. Extended rheology sweep: a more realistic rheological approach to investigate the process of mucoadhesive polymer-mucus gel chain interpenetration. *Iranian Pol. J.*, 12:413–420, 2003.
- [42] H. R. Morton and S. Grishanov. Doubly periodic textile structures. *J. Knot Theory Ramif.*, 18:1597–1622, 2009.

- [43] H. C. Öttinger. *Beyond equilibrium thermodynamics*. Wiley, Hoboken, 2005.
- [44] E. Panagiotou. The linking number in systems with periodic boundary conditions. *J. Comput. Phys.*, 300:533–573, 2015.
- [45] E. Panagiotou and M. Kröger. Pulling-force-induced elongation and alignment effects on entanglement and knotting characteristics of linear polymers in a melt. *Phys. Rev. E*, 90:042602, 2014.
- [46] E. Panagiotou, M. Kröger, and K. C. Millett. Writhe and mutual entanglement combine to give the entanglement length. *Phys. Rev. E*, 88:062604, 2013.
- [47] E. Panagiotou, C. Tzoumanekas, S. Lambropoulou, K. C. Millett, and D. N. Theodorou. A study of the entanglement in systems with periodic boundary conditions. *Progr. Theor. Phys. Suppl.*, 191:172–181, 2011.
- [48] S. J. Park, P. S. Desai, X. Chen, and R. G. Larson. Universal relaxation behavior of entangled 1,4-polybutadiene melts in the transition frequency region. *Macromolecules*, 48:4122–4131, 2015.
- [49] S. Plimpton. Fast parallel algorithms for short-range molecular dynamics. *J. Comput. Phys.*, 117:1–19, 1995.
- [50] J. Qin and S. T. Milner. Counting polymer knots to find the entanglement length. *Soft Matter*, 7:10676–93, 2011.
- [51] M. E. Rosa and H. H. Winter. The effect of entanglement on the rheological behavior of polybutadiene critical gels. *Rheo. Acta*, 33:220–237, 1994.
- [52] S. B. Ross-Murphy and H. McEvoy. Fundamentals of hydrogels and gelatin. *Br. Polym. J.*, 18:2–7, 1986.
- [53] M. Rubinstein and R. Colby. *Polymer Physics*. Oxford University Press, 2003.
- [54] M. Rubinstein and E. J. Helfand. Statistics of entanglements of polymers: Concentration effects. *J. Chem. Phys.*, 82:2477–2483, 1984.
- [55] S. Saito, T. Hashimoto, I. Morfin, P. Lindner, F. Boué, and D. J. Pine. Phase separation in a polymer solution induced by theady and large amplitude oscillatory shear flow. *Macromolecules*, 36:3745–3748, 2003.
- [56] S. Shanbhag and M. Kröger. Primitive path networks generated by annealing and geometrical methods: Insights into differences. *Macromolecules*, 40:2897, 2007.
- [57] Z. Shen, M. Röding, M. Kröger, and Y. Li. Carbon nanotube length governs the viscoelasticity and permeability of buckypaper. *Polymers*, 9:9040115, 2017.
- [58] P. S. Stephanou, C. Baig, G. Tsolou, V. G. Mavrantzas, and M. Kröger. Quantifying chain reptation in entangled polymer melts. *J. Chem. Phys.*, 132:124904, 2010.

- [59] D. M. Sussman and K. S. Schweizer. Microscopic theory of entangled polymer melt dynamics: flexible chains as primitive-path random walks and supercoarse grained needles. *PRL*, 109:168306, 2012.
- [60] L. Szántó, R. Vogt, J. Meier, D. Auhl, E. Van Ruymbeke, and C. Friedrich. Entanglement relaxation time of polyethylene melts from high-frequency rheometry in the mega-hertz range. *J. Rheol.*, 61:1023, 2017.
- [61] V. Trappe and D. A. Weitz. Scaling of the viscoelasticity of weakly attractive particles. *Phys. Rev. Lett.*, 85:449–452, 2000.
- [62] C. Tzoumanekas and D. N. Theodorou. Topological analysis of linear polymer melts: a statistical approach. *Macromolecules*, 39:4592–4604, 2006.
- [63] H. J. Unidad, M. A. Goad, A. R. Bras, M. Zamponi, R. Faust, J. Allgaier, W. Pyckhout-Hintzen, A. Wischnewski, D. Richter, and L. J. Fetters. Consequences of increasing packing length of the dynamics of polymer melts. *Macromolecules*, 48:6638–6645, 2015.
- [64] Y. Wang, J. K. Sigurdsson, and P. J. Atzberger. Fluctuating hydrodynamics methods for dynamic coarse-grained implicit-solvent simulations in lammmps. *SIAM Journal on Scientific Computing*, 38(5):S62–S77, 2016.
- [65] M. Wilson, A. Rabinovitch, and A. R. C. Baljon. Computational study of the structure and rheological properties of self-associating polymer networks. *Macromolecules*, 48:6313–6320, 2015.
- [66] R. Yu, C. Zhou, and J. J. Feng. Rheology and relaxation processes in a melting thermotropic liquid-crystalline polymer. *J. Applied Pol Science*, 104:3780–3787, 2006.